

# The Fubini-Furlan-Rossetti Sum Rule Revisited

B. Pasquini<sup>1</sup>, D. Drechsel<sup>2</sup>, L. Tiator<sup>2</sup>

<sup>1</sup> Dipartimento di Fisica Nucleare e Teorica, Università degli Studi di Pavia; INFN, Sezione di Pavia, Pavia, Italy, and ECT\*, Villazzano (Trento), Italy,

<sup>2</sup> Institut für Kernphysik, Johannes Gutenberg-Universität, D-55099 Mainz

Received: date / Revised version: date

**Abstract** The Fubini-Furlan-Rossetti sum rule for pion photoproduction on the nucleon is evaluated by dispersion relations at constant  $t$ , and the corrections to the sum rule due to the finite pion mass are calculated. Near threshold these corrections turn out to be large due to pion-loop effects, whereas the sum rule value is closely approached if the dispersion integrals are evaluated for sub-threshold kinematics. This extension to the unphysical region provides a unique framework to determine the low-energy constants of chiral perturbation theory by global properties of the excitation spectrum.

## 1 Introduction

The Fubini-Furlan-Rossetti (FFR) sum rule was derived on the basis of current algebra and PCAC in the soft-pion limit [1]. It relates the anomalous magnetic moment to single-pion photoproduction on the nucleon. By use of the Goldberger-Treiman relation [2] the sum rule takes the form

$$\kappa^{V,S} = \frac{8M_N^2}{e\pi g_{\pi N}} \int \frac{d\nu'}{\nu'} \text{Im} A_1^{(+,0)}(\nu', t=0), \quad (1)$$

with  $\kappa^V = \kappa_p - \kappa_n = 3.706$  and  $\kappa^S = \kappa_p + \kappa_n = -0.120$  the isovector and isoscalar anomalous magnetic moments, and  $A_1^{(+,0)}$  the respective combinations of the first invariant amplitude of pion photoproduction. Furthermore,  $M_N$  is the nucleon mass,  $M_\pi$  the mass of the neutral pion, and  $g_{\pi N}$  the pseudoscalar pion-nucleon coupling constant. The imaginary part of the amplitude  $A_1^{(+,0)}$  is evaluated at small momentum transfer  $t$ , and the crossing-symmetrical variable  $\nu'$  approaches the photon lab energy in the soft-pion limit ( $M_\pi \rightarrow 0$ ,  $t \rightarrow 0$ ). In their derivation the authors of Ref. [1] tacitly assume that the RHS of Eq. (1) is evaluated in the chiral limit of massless pions. However, the finite mass corrections contained in the experimental data for  $\text{Im} A_1^{(+,0)}$  will yield deviations from the sum rule value, even though the suggested path of integration at  $t = 0$  (corresponding to forward production of massless pions) is expected to minimize these corrections.

The isovector sum rule was found to be slightly over-predicted in 1966 by a then existing model of  $\Delta(1232)$  resonance excitation [3]. Adler and Gilman [4] generalized the sum rule to pion electroproduction and evaluated the RHS of Eq. (1) with an early multipole analysis [5]. While the  $\Delta(1232)$  multipoles yielded only about 60% of the sum rule value, the non-resonant S-wave multipoles contributed another 25%. The authors of Ref. [4]

derived the sum rule in the limit of vanishing values for  $\nu$ ,  $\nu_B$ , and  $M_\pi^2$ , where  $\nu_B = (t - M_\pi^2)/4M_N$  and  $\nu = \pm\nu_B$  gives the position of the nucleon poles. The soft pion limit was approached by first letting  $\nu_B \rightarrow 0$  and then setting  $\nu = 0$ , and the lower limit of the integral was fixed at  $\nu' = \nu_B + M_\pi + M_\pi^2/(2M_N)$ .

In a more recent investigation Arndt and Workman [6] used the VPI data basis and obtained the values 3.92 and  $-0.138$  from the RHS of Eq. (1) for  $\kappa^V$  and  $\kappa^S$ , respectively.

The FFR sum rule relies on two basic assumptions. First, the amplitudes  $A_1^{(+,0)}$  have to be evaluated at the origin of the Mandelstam plane,  $\nu = \nu_B = t = 0$ , which also requires that the pion mass vanishes. In this point of the Mandelstam plane the pole terms due to the Dirac current vanish, and the only contribution stems from the Pauli current, which yields a constant (non-pole) contribution proportional to the anomalous magnetic moment (LHS of Eq. (1)). It is thereby assumed that all terms beyond the nucleon pole graphs vanish at  $\nu = t = M_\pi = 0$ . The second assumption concerns the integral on the RHS of Eq. (1), which is evaluated by means of dispersion relations at  $t = \text{const}$ . In order to describe the amplitude at  $\nu = t = 0$ , the imaginary part under the integral therefore should be evaluated at  $t = 0$ , which for  $M_\pi \neq 0$  is outside the physical region of the Mandelstam plane. The closest approximation to  $t = 0$  is forward pion production,  $\theta = 0$ , which then requires an extrapolation of the amplitude from  $t(\nu, \theta) < 0$  to  $t = 0$ .

It is the aim of this work to investigate the FFR sum rule at  $t = t_{\text{thr}}$ , which yields the only path of integration that is completely within the physical region (see Fig. 1). The salient features of both kinematics and photoproduction amplitudes are given in the following section 2. The extrapolation to the soft-pion limit ( $M_\pi \rightarrow 0$ ) requires, of course, a dynamical framework. For this purpose we

outline the predictions of heavy baryon chiral perturbation theory (HBChPT) in section 3. These predictions are compared to the results of dispersion relations (DRs) based on MAID03 in section 4. We present our results for the dispersion integrals at  $t = t_{\text{thr}}$  as function of  $\nu$ , which near threshold ( $\nu = \nu_{\text{thr}}$ ) yield large cusp effects from loop corrections but decrease rapidly with decreasing  $\nu$  and pass through a zero at  $\nu \approx 70$  MeV. A comparison of our approach with HBChPT shows good agreement in the threshold region. However, the nonrelativistic approximations of HBChPT turn out to be problematic in the unphysical region far below pion threshold. Our findings confirm the necessity to provide a fully relativistic treatment of ChPT, and at the same time they yield a framework to determine the low-energy constants (LECs) of such a theory by global properties of the nucleon's excitation spectrum. In section 5 we close with a short summary and an outlook.

## 2 Pion Photoproduction Amplitudes

Let us first define the kinematics of pion photoproduction on a nucleon, the reaction

$$\gamma(k) + N(p_i) \rightarrow \pi(q) + N'(p_f),$$

where the variables in brackets denote the four-momenta of the participating particles. The familiar Mandelstam variables are

$$s = (p_i + k)^2, \quad t = (q - k)^2, \quad u = (p_i - q)^2, \quad (2)$$

and

$$\nu = (s - u)/4M_N \quad (3)$$

is the crossing symmetrical variable. This variable is related to the photon lab energy  $E_\gamma^{lab}$  by

$$\nu = E_\gamma^{lab} + \frac{t - M_\pi^2}{4M_N}. \quad (4)$$

The physical s-channel region is shown in Fig. 1. Its upper and lower boundaries are given by the scattering angles  $\theta = 0$  and  $\theta = 180^\circ$ , respectively. The nucleon and pion poles lie in the unphysical region and are indicated by the dotted lines at  $\nu_s = \nu_B$  (s-channel) and  $\nu_u = -\nu_B$  (u-channel), where

$$\nu_B = \frac{t - M_\pi^2}{4M_N}. \quad (5)$$

The threshold for pion photoproduction lies at

$$\begin{aligned} \nu_{\text{thr}} &= \frac{M_\pi(2M_N + M_\pi)^2}{4M_N(M_N + M_\pi)}, \\ t_{\text{thr}} &= -\frac{M_\pi^2 M_N}{M_N + M_\pi}. \end{aligned} \quad (6)$$

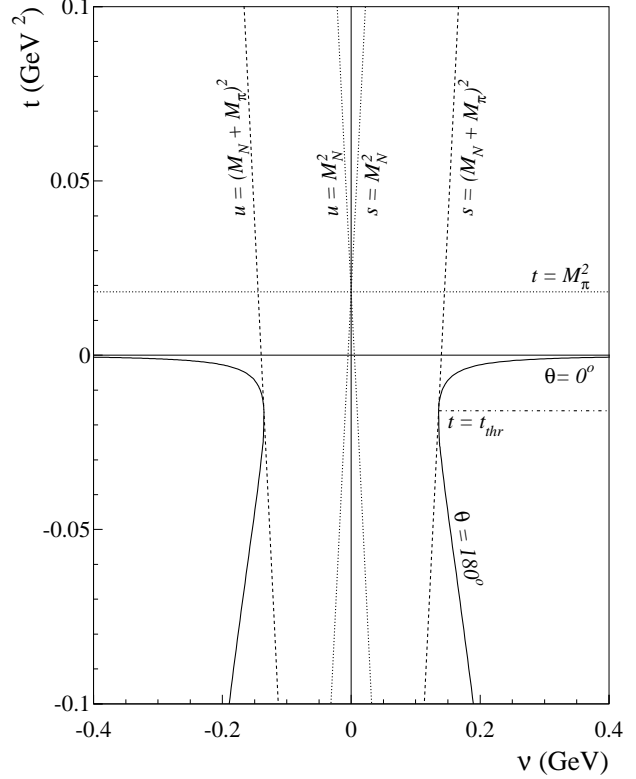


**Figure 1.** The Mandelstam plane for pion photoproduction on the nucleon. The boundaries of the physical region are  $\theta = 0$  (forward production) and  $\theta = 180^\circ$  (backward production). The nucleon and pion pole positions are indicated by the dotted lines  $s = M_N^2$ ,  $u = M_N^2$ , and  $t = M_\pi^2$ . The dashed line  $s = (M_N + M_\pi)^2$  indicates the threshold of pion production and therefore also of the imaginary part of the production amplitude. It is tangent to the boundary of the physical region in the point  $\nu = \nu_{\text{thr}}$ ,  $t = t_{\text{thr}}$ . The path of integration starting in that point (dashed-dotted line) yields the only dispersion relation at  $t = \text{const}$  whose imaginary part is fully contained in the physical region.

In the pion-nucleon center-of-mass (c.m.) system, we have

$$\begin{aligned} p_i^\mu &= (E_i, -\mathbf{k}), & p_f^\mu &= (E_f, -\mathbf{q}), \\ \mathbf{k}^\mu &= (|\mathbf{k}|, \mathbf{k}), & \mathbf{q}^\mu &= (\omega, \mathbf{q}), \end{aligned} \quad (7)$$

where

$$\begin{aligned} k &= |\mathbf{k}| = \frac{s - M_N^2}{2\sqrt{s}}, & \omega &= \frac{s + M_\pi^2 - M_N^2}{2\sqrt{s}}, \\ q &= |\mathbf{q}| = \left[ \left( \frac{s + M_\pi^2 - M_N^2}{2\sqrt{s}} \right)^2 - M_\pi^2 \right]^{1/2} \\ &= \left[ \left( \frac{s - M_\pi^2 + M_N^2}{2\sqrt{s}} \right)^2 - M_N^2 \right]^{1/2}, \\ E_i &= W - k = \frac{s + M_N^2}{2\sqrt{s}} \end{aligned}$$

$$E_f = W - \omega = \frac{s + M_N^2 - M_\pi^2}{2\sqrt{s}}, \quad (8)$$

with  $W = \sqrt{s}$  the c.m. energy.

The nucleon electromagnetic current can be expressed in terms of 4 invariant amplitudes  $A_i$  [7,8],

$$J^\mu = \sum_i A_i(\nu, t) M_i^\mu, \quad (9)$$

with the four-vectors  $M_i^\mu$  given by

$$\begin{aligned} M_1^\mu &= -\frac{1}{2}i\gamma_5(\gamma^\mu \not{k} - \not{k}\gamma^\mu), \\ M_2^\mu &= 2i\gamma_5(P^\mu k \cdot q - q^\mu k \cdot P), \\ M_3^\mu &= -i\gamma_5(\gamma^\mu k \cdot q - \not{k}q^\mu), \\ M_4^\mu &= -2i\gamma_5(\gamma^\mu k \cdot P - \not{k}P^\mu) - 2M_N M_1^\mu, \end{aligned} \quad (10)$$

where  $P^\mu = (p_f^\mu + p_i^\mu)/2$  and the gamma matrices are defined as in Ref. [9].

The invariant amplitudes  $A_i$  can be further decomposed into three isospin channels ( $a = 1, 2, 3$ ),

$$A_i^a = A_i^{(-)}i\epsilon^{a3b}\tau^b + A_i^{(0)}\tau^a + A_i^{(+)}\delta_{a3}, \quad (11)$$

where  $\tau^a$  are the Pauli matrices in isospace. The physical photoproduction amplitudes are then obtained from the following linear combinations:

$$\begin{aligned} A_i(\gamma p \rightarrow n\pi^+) &= \sqrt{2}(A_i^{(-)} + A_i^{(0)}), \\ A_i(\gamma p \rightarrow p\pi^0) &= A_i^{(+)} + A_i^{(0)}, \\ A_i(\gamma n \rightarrow p\pi^-) &= -\sqrt{2}(A_i^{(-)} - A_i^{(0)}), \\ A_i(\gamma n \rightarrow n\pi^0) &= A_i^{(+)} - A_i^{(0)}. \end{aligned} \quad (12)$$

The FFR sum rule is derived from the pion-photoproduction amplitude in the limit of  $q^\mu \rightarrow 0$ . As we note from Eq. (10), the four-vectors  $M_2^\mu$ ,  $M_3^\mu$ , and  $M_4^\mu$  vanish, and only the four-vector  $M_1^\mu$  survives in that limit.

The isospin amplitudes  $A_1^I$  satisfy the following dispersion relation at fixed  $t$ :

$$\text{Re}A_1^{(+,0)}(\nu, t) = \quad (13)$$

$$A_1^{(+,0)pole}(\nu, t) + \frac{2}{\pi}\mathcal{P} \int_{\nu_{thr}}^{\infty} d\nu' \frac{\nu' \text{Im}A_1^{(+,0)}(\nu', t)}{\nu'^2 - \nu^2},$$

$$\text{Re}A_1^{(-)}(\nu, t) = \quad (14)$$

$$A_1^{(-)pole}(\nu, t) + \frac{2\nu}{\pi}\mathcal{P} \int_{\nu_{thr}}^{\infty} d\nu' \frac{\text{Im}A_1^{(-)}(\nu', t)}{\nu'^2 - \nu^2}.$$

Similar relations may be obtained for the amplitudes  $A_2 - A_4$  [10,8].

The nucleon pole contributions  $A_i^{I,pole}$  ( $I = 0, +, -$ ) are given by

$$\begin{aligned} A_1^{I,pole} &= \frac{eg_{\pi N}}{2} \left( \frac{1}{s - M_N^2} + \frac{\epsilon^I}{u - M_N^2} \right), \\ A_2^{I,pole} &= -\frac{eg_{\pi N}}{t - m_\pi^2} \left( \frac{1}{s - M_N^2} + \frac{\epsilon^I}{u - M_N^2} \right), \end{aligned}$$

$$A_3^{I,pole} = -\frac{eg_{\pi N}}{2m_N} \frac{\kappa^I}{2} \left( \frac{1}{s - M_N^2} - \frac{\epsilon^I}{u - M_N^2} \right),$$

$$A_4^{I,pole} = -\frac{eg_{\pi N}}{2m_N} \frac{\kappa^I}{2} \left( \frac{1}{s - M_N^2} + \frac{\epsilon^I}{u - M_N^2} \right), \quad (15)$$

with  $\epsilon^+ = \epsilon^0 = -\epsilon^- = 1$ ,  $\kappa^{(+,-)} = \kappa_p - \kappa_n$ , and  $\kappa^{(0)} = \kappa_p + \kappa_n$ , where  $\kappa_p$  and  $\kappa_n$  are the anomalous magnetic moments of the proton and the neutron, respectively. The nucleon pole contributions are most easily constructed by evaluating the tree-level diagrams with the pseudoscalar pion-nucleon coupling. We note in particular that the amplitudes  $A_1^{I,pole}$  and  $A_2^{I,pole}$  are independent of the anomalous magnetic moment  $\kappa_N$  of the respective nucleon, whereas the amplitudes  $A_3^{I,pole}$  and  $A_4^{I,pole}$  are proportional to  $\kappa_N$ . In order to obtain the proper chiral structure, the tree-level contribution is calculated with pseudovector (PV) coupling, and the amplitudes  $A_1^{(+,0)}$  change according to

$$A_1^{(+,0)PV} = A_1^{(+,0)pole} + A_1^{(+,0)FFR}, \quad (16)$$

where

$$A_1^{(+,0)FFR} = \frac{eg_{\pi N} \kappa^{(+,0)}}{4M_N^2}. \quad (17)$$

All other amplitudes remain unchanged.

The covariant amplitude  $A_1$  can be expressed by the CGLN amplitudes [7,8]  $\mathcal{F}_i$  ( $i = 1 \dots 4$ ) as follows:

$$\begin{aligned} A_1 &= \frac{4\pi}{\sqrt{(E_i + M_N)(E_f + M_N)}} \quad (18) \\ &\left\{ \frac{W + M_N}{W - M_N} \mathcal{F}_1 - (E_f + M_N) \frac{\mathcal{F}_2}{q} \right. \\ &\left. + \frac{M_N(t - M_\pi^2)}{(W - M_N)^2} \frac{\mathcal{F}_3}{q} + \frac{M_N(E_f + M_N)(t - M_\pi^2)}{W^2 - M_N^2} \frac{\mathcal{F}_4}{q^2} \right\}, \end{aligned}$$

where  $q = |\mathbf{q}|$  and all variables are expressed in the c.m. frame. Below the  $\Delta(1232)$  resonance, we may limit ourselves to the S-wave multipole and to the three P-wave multipoles  $E_{1+}$ ,  $M_{1+}$ , and  $M_{1-}$ . In this approximation, the CGLN amplitudes take the form

$$\begin{aligned} \mathcal{F}_1 &\rightarrow E_{0+} + 3(M_{1+} + E_{1+}) \cos \theta, \\ \mathcal{F}_2/q &\rightarrow (2M_{1+} + M_{1-})/q, \\ \mathcal{F}_3/q &\rightarrow 3(E_{1+} - M_{1+})/q, \quad \mathcal{F}_4 \rightarrow 0, \end{aligned} \quad (19)$$

where  $\theta$  is the c.m. scattering angle, which is related to the Mandelstam variables by

$$\cos \theta = \frac{(s - M_N^2)^2 - M_\pi^2(s + M_N^2) + 2st}{2q\sqrt{s}(s - M_N^2)}. \quad (20)$$

The P-wave contributions are often expressed by the three combinations

$$\begin{aligned} P_1 &= 3E_{1+} + M_{1+} - M_{1-}, \\ P_2 &= 3E_{1+} - M_{1+} + M_{1-}, \\ P_3 &= 2M_{1+} + M_{1-}. \end{aligned} \quad (21)$$

With these definitions the multipole expansion of Eq. (18) can be cast into the form

$$A_1 = \frac{4\pi(W + M_N)}{\sqrt{(E_i + M_N)(E_f + M_N)}(W - M_N)} \quad (22)$$

$$\left\{ E_{0+} + \left( \omega + \frac{W(t - M_\pi^2)}{W^2 - M_N^2} \right) \bar{P}_1 \right. \\ \left. + \frac{M_N(t - M_\pi^2)}{W^2 - M_N^2} \bar{P}_2 + \frac{t}{W + M_N} \bar{P}_3 + \dots \right\},$$

with  $\bar{P}_i = P_i/q$  and the ellipses denoting the higher partial waves.

The FFR sum rule follows in the limit  $q^\mu \rightarrow 0$ , which we approach by first going to the production threshold ( $\mathbf{q} = 0$  in the c.m. frame) and then letting  $M_\pi \rightarrow 0$ . In the limit  $q = |\mathbf{q}| \rightarrow 0$ , only the S-wave multipole  $E_{0+}$ , the slopes of the P-wave multipoles, and the curvatures of the D-wave multipoles contribute to Eq. (22). Furthermore, the kinematical factors simplify at threshold, and Eq. (22) takes the form

$$A_1(\nu_{thr}, t_{thr}) = \frac{4\pi}{M_\pi} \sqrt{\frac{M_N + M_\pi}{M_N}} \quad (23)$$

$$\left\{ E_{0+} - \frac{M_N M_\pi}{M_N + M_\pi} \bar{P}_2 - \frac{M_N M_\pi^2}{(2M_N + M_\pi)(M_N + M_\pi)} \right. \\ \left. (\bar{P}_3 + 6M_N \bar{D}) \right\},$$

where  $\bar{D} = (M_{2+} - E_{2+} - M_{2-} - E_{2-})/q^2$ , and all the multipoles have to be evaluated at  $q = 0$ . In particular we note that the amplitude  $\bar{P}_1$  does not appear in Eq. (23), because its kinematical prefactor vanishes at threshold.

With these definitions it is straightforward to obtain the threshold value of the invariant amplitude, Eq. (23), from current multipole analyses or chiral perturbation theory (ChPT). The second step involved in the FFR, the extrapolation to  $M_\pi = 0$ , can of course only be performed within a theoretical framework like ChPT.

### 3 Predictions of HBChPT

The Born terms in ChPT are evaluated with pseudovector pion-nucleon coupling in order to obtain the correct chiral threshold behavior. The additional loop and counterterm contributions to the S- and P-wave amplitudes have been predicted by HBChPT to fourth order in  $1/M_N$  [11,12,13]. After subtraction of the nucleon-pole terms given in Appendix A, we find the following amplitude for neutral pion photoproduction on a nucleon  $N$ :

$$A_1(\nu, t) - A_1^{pole}(\nu, t) = \frac{e g_{\pi N}}{2M_N^2} \kappa_N \tau_3 + A_1^{\text{loop}}(\nu, t) + A_1^{\text{ct}}(\nu, t), \quad (24)$$

where use has been made of Eqs. (12), (16), and (17). In Eq. (24),  $\kappa_N \tau_3$  takes the values 1.793 for the proton and 1.913 for the neutron. The appearance of the anomalous

magnetic moment  $\kappa_N$  in this expression is, of course, the essence of the FFR sum rule.

Because the FFR term of Eq. (17) is a constant, the associated current contributes only to the partial waves  $E_{0+}$  and  $M_{1-}$ ,

$$E_{0+}^{\text{FFR}} = \frac{e g_{\pi N} \kappa_N \tau_3}{2M^2} \quad (25)$$

$$\frac{W + M_N}{8\pi W} \sqrt{\frac{E_f + M}{E_i + M}} \frac{W^2 - M_N^2}{2W},$$

$$\bar{M}_{1-}^{\text{FFR}} = -\frac{e g_{\pi N} \kappa_N \tau_3}{2M^2}$$

$$\frac{W + M_N}{8\pi W} \frac{1}{\sqrt{(E_i + M)(E_f + M)}} \frac{W^2 - M_N^2}{2W}.$$

Both contributions are proportional to the photon energy  $k$  that vanishes at the nucleon pole position  $W = M_N$ . Reconstructing  $A_1^{\text{FFR}}$  from its multipoles by Eq. (22), one finds that the sum of the P-wave contributions vanishes at the pole position, despite the denominators  $(W - M_N)^{-2}$  in that equation. As a consequence, only the S-wave contributes to  $A_1^{\text{FFR}}$  at the nucleon poles.

While the tree diagrams can be calculated exactly, HBChPT provides the loop and counterterm contributions as the first terms of a power series in the pion energy  $\omega$  [11,13]. In particular, the loop contributions to the S- and P-wave multipoles at threshold,  $\omega = M_\pi$ , are given by

$$E_{0+}^{\text{loop}}(\omega_{thr}) = \frac{e g_A M_\pi^2}{128\pi F_\pi^3} + \frac{e g_A M_\pi^3}{72\pi^3 F_\pi^3 M_N}$$

$$\left\{ -1 - \frac{45\pi^2}{64} + \frac{33}{8} \ln \frac{M_\pi}{\lambda} + \tau_3 \left( -\frac{5}{4} + \frac{3}{2} \ln \frac{M_\pi}{\lambda} \right) \right\}$$

$$- \frac{e g_A^3 M_\pi^3}{512\pi^3 F_\pi^3 M_N} \left( \frac{44}{9} - \frac{20}{3} \pi + \pi^2 - \frac{32}{3} \ln \frac{M_\pi}{\lambda} \right), \quad (26)$$

$$\bar{P}_1^{\text{loop}}(\omega_{thr}) = \frac{e g_A^3 M_\pi}{384\pi^2 F_\pi^3} (10 - 3\pi) + \frac{e g_A M_\pi^2}{512\pi^3 F_\pi^3 M_N}$$

$$\left\{ 16 + \pi^2 + 24 \ln \frac{M_\pi}{\lambda} + \tilde{c}_4 \left[ \frac{32}{9} + \frac{64}{3} \ln \frac{M_\pi}{\lambda} \right] \right\}$$

$$+ \frac{e g_A^3 M_\pi^2}{2304\pi^3 F_\pi^3 M_N} \left\{ 20 - 2(\kappa_n - \kappa_p) - 30\pi + 9\pi^2 \right. \\ \left. + 6\tau_3(1 + \kappa_n + \kappa_p) \right. \\ \left. + 12[4 - \kappa_n + \kappa_p + 3\tau_3(1 + \kappa_n + \kappa_p)] \ln \frac{M_\pi}{\lambda} \right\}, \quad (27)$$

$$\bar{P}_2^{\text{loop}}(\omega_{thr}) = -\frac{e g_A^3 M_\pi}{192\pi^2 F_\pi^3} - \frac{e g_A M_\pi^2}{256\pi^3 F_\pi^3 M_N}$$

$$\left\{ -4 + \left( \pi^2 - \frac{80}{9} \right) 2\tilde{c}_4 + \pi^2 + \left( 8 + \frac{16}{3} \tilde{c}_4 \right) \ln \frac{M_\pi}{\lambda} \right\}$$

$$+ \frac{e g_A^3 M_\pi^2}{192\pi^3 F_\pi^3 M_N} \left\{ \frac{\pi}{2} - \frac{3}{8} \pi^2 + \frac{11}{6} + \frac{2}{3} \kappa_n + \frac{1}{3} \kappa_p \right. \\ \left. - \frac{1}{2} (1 + \tau_3)(1 + \kappa_n + \kappa_p) - [4 - 2\kappa_p - 4\kappa_n \right. \\ \left. + 3(1 + \tau_3)(1 + \kappa_n + \kappa_p)] \ln \frac{M_\pi}{\lambda} \right\}, \quad (28)$$

$$\begin{aligned} \bar{P}_3^{\text{loop}}(\omega_{\text{thr}}) &= -\frac{eg_A M_\pi^2}{256\pi F_\pi^3 M_N}(1 + 4\tilde{c}_4) \\ &\quad -\frac{eg_A^3 M_\pi^2}{192\pi^2 F_\pi^3 M_N}\{2(1 - \kappa_n + \kappa_p) + \tau_3(1 + \kappa_n + \kappa_p)\}, \end{aligned} \quad (29)$$

where the low energy constant  $\tilde{c}_4 = M_N c_4$  with  $c_4 = 3.4 \text{ GeV}^{-1}$ . The scale of dimensional regularization is set equal to the nucleon mass,  $\lambda = M_N$ . Furthermore the axial coupling constant  $g_A$  is fixed through the Goldberger-Treiman relation,  $g_A = g_{\pi N} F_\pi / M_N$  with  $g_{\pi N} = 13.1$  and  $F_\pi = 92.4 \text{ MeV}$ .

The counterterm contributions at threshold take the form [11, 13]

$$E_{0+}^{\text{ct}}(\omega_{\text{thr}}) = e(a_1^{p,n}(\lambda) + a_2^{p,n}(\lambda)) M_\pi^3, \quad (30)$$

$$\bar{P}_{1,2}^{\text{ct}}(\omega_{\text{thr}}) = \frac{eg_A M_\pi^2}{64\pi^3 F_\pi^3 M_N} \xi_{1,2}^{p,n}(\lambda), \quad (31)$$

$$\bar{P}_3^{\text{ct}}(\omega_{\text{thr}}) = e b_P^{p,n} \left\{ M_\pi - \frac{M_\pi^2}{2M_N} \right\}, \quad (32)$$

where the low-energy constants have been either fitted to the threshold data or estimated as the sum of vector meson exchange and  $\Delta$  resonance contributions by use of the resonance saturation principle (see Appendix B).

By use of Eq. (24), the dispersion relation of Eq. (13) can be cast into the form

$$\begin{aligned} \kappa_N \tau_3 + \frac{2M_N^2}{eg_{\pi N}} \left\{ A_1^{\text{loop}}(\nu, t_{\text{thr}}) + A_1^{\text{ct}}(\nu, t_{\text{thr}}) \right\} \\ = \frac{4M_N^2}{\pi e g_{\pi N}} \mathcal{P} \int_{\nu_{\text{thr}}}^{\infty} d\nu' \frac{\nu' \text{Im} A_1^{(N,\pi^0)}(\nu', t_{\text{thr}})}{\nu'^2 - \nu^2}, \end{aligned} \quad (33)$$

If we insert Eqs. (26)-(32) into Eq. (23), we find immediately that the loop and counterterm contributions in the curly bracket of Eq. (33) vanish in the soft-pion limit,  $M_\pi \rightarrow 0$ , which also leads to  $\nu_{\text{thr}} \rightarrow 0$  and  $t_{\text{thr}} \rightarrow 0$ . This result is in agreement with a low-energy theorem derived on the basis of PCAC [4] and has also been proved at the one-loop order in relativistic ChPT [15]. The result is the FFR sum rule,

$$\kappa_N \tau_3 = \frac{4M_N^2}{\pi e g_{\pi N}} \int_0^\infty d\nu' \frac{\text{Im} A_1^{(N,\pi^0)}(\nu', 0)}{\nu'}. \quad (34)$$

Of course, the imaginary part of the amplitudes in the dispersion integral becomes a theoretical construct in the limit that describes the world of massless pions. In order to stay in contact with the experimental data, our strategy is to evaluate the RHS of Eq. (33) along  $t = t_{\text{thr}}$  and to study the loop and counterterm corrections as function of  $\nu$ . Figure 1 shows that this is the only path  $t = \text{const}$  for which  $\text{Im} A_1$  is directly related to the experimental data, whereas all the other paths require an extrapolation into unphysical regions of the Mandelstam plane. For further

discussion we define the finite mass corrections  $\Delta_N$  to the FFR sum rule by the following equations:

$$\begin{aligned} \Delta_N(\nu, t_{\text{thr}}) &= \\ &\quad \frac{2M_N^2}{eg_{\pi N}} \left\{ A_1^{\text{loop}}(\nu, t_{\text{thr}}) + A_1^{\text{ct}}(\nu, t_{\text{thr}}) \right\}, \end{aligned} \quad (35)$$

$$\begin{aligned} \kappa_N \tau_3 + \Delta_N(\nu, t_{\text{thr}}) &= \\ &\quad \frac{4M_N^2}{\pi e g_{\pi N}} \mathcal{P} \int_{\nu_{\text{thr}}}^{\infty} d\nu' \frac{\nu' \text{Im} A_1^{(N,\pi^0)}(\nu', t_{\text{thr}})}{\nu'^2 - \nu^2}. \end{aligned} \quad (36)$$

We recall that the lower limit  $\nu_{\text{thr}}$  of the dispersion integral is the threshold for neutral pion photoproduction. In practice, however, the imaginary parts of the amplitudes are negligible below the onset of charged pion production, which yields a strong cusp effect due to the large imaginary part of the S-wave amplitudes.

## 4 Results

In order to obtain the correction  $\Delta_N(\nu, t_{\text{thr}})$  due to the physical pion mass, we evaluate the invariant amplitude  $A_1^{(N,\pi^0)}$  of Eq. (33) with the multipoles as predicted by HBChPT, whereas the dispersion integral of Eq. (33) is evaluated with the MAID03 result for the imaginary part of the  $A_1^{(N,\pi^0)}$  amplitude.

In Table 1 we collect the results for the FFR sum rule of the proton and neutron channels. The first column shows the experimental values of  $\kappa_p$  and  $-\kappa_n$ , the second column includes the finite mass corrections at pion threshold as calculated from the loop and counterterms of HBChPT (Eq. (33)). The results obtained from the dispersion integral (RHS of Eq. (33)) are shown for  $\nu = \nu_{\text{thr}}$  in the third column and for  $\nu = 0$  in the last column.

Both the HBChPT and the dispersion predictions yield large finite-mass corrections at threshold. In the case of the proton we find  $\Delta_p(\nu_{\text{thr}}, t_{\text{thr}}) \approx 0.5$ , in good agreement between HBChPT and DR. The corresponding corrections for the neutron turn out to be somewhat larger and take values of about 0.65. However it turns out that the corrections  $\Delta_N$  have become small and negative for  $\nu = 0$ .

Table 2 compares the experimental threshold values for the lowest multipoles to the results of several theoretical descriptions. The latter include the phenomenological model MAID03 [16], the dispersion analysis HDT [8], and the dynamical (Dubna-Mainz-Taipei) model [17]. Concerning the comparison with the predictions of HBChPT, we note that we have used the charged pion mass in all the loops and counterterms, and evaluated the LECs with the  $\Delta(1232)$  parameters given in Appendix B. Occasionally, this leads to a slight difference between the numbers in Tab. 2 and those given in Refs. [11, 12, 13], which however is irrelevant for our further discussion. In the case of  $E_{0+}^p$  we find a good agreement between HBChPT and the phenomenological models, however there are some deviations for the proton P-wave multipoles. Concerning the higher partial waves, only a particular combination of the

	FFR	HBChPT ( $\nu = \nu_{\text{thr}}$ )	DR ( $\nu = \nu_{\text{thr}}$ )	DR ( $\nu = 0$ )
proton	1.793	2.29/2.33/2.37	2.24	1.66
neutron	1.913	2.52/2.56/2.79	2.44	1.82

**Table 1.** The FFR sum rule for proton and neutron. First column: sum rule values in the limit of  $M_\pi \rightarrow 0$ . Second column: LHS of Eq. (33) as obtained from the HBChPT predictions for the S- and P-wave multipoles evaluated at  $\nu = \nu_{\text{thr}}$ . The results are given with the LECs listed in Appendix B according to Refs. [11], [12], and [13], in order. Third column: dispersion prediction for the RHS of Eq. (33) at  $\nu = \nu_{\text{thr}}$  evaluated with MAID03. Fourth column: dispersion prediction for the RHS of Eq. (33) at  $\nu = 0$  evaluated with MAID03.

	pole	MAID03/HDT/DMT	HBChPT	experiment
$E_{0+}^p$	-7.89	-1.27/ - 1.22/ - 1.16	-1.23/ - 1.15/ - 1.12	$-1.23 \pm 0.08 \pm 0.03$
$\bar{P}_1^p$	8.74	9.35/9.64/9.31	9.35/9.12/8.37	$9.46 \pm 0.05 \pm 0.28$
$\bar{P}_2^p$	-8.51	-10.87/ - 10.49/ - 10.15	-9.88/ - 9.61/ - 9.63	$-9.5 \pm 0.09 \pm 0.28$
$\bar{P}_3^p$	0.59	7.43/9.38/9.23	12.90/10.63/5.90	$11.32 \pm 0.11 \pm 0.34$
$D^p$	1.00	0.96/ - /0.92	-	-
$E_{0+}^n$	-5.44	1.47/1.19/1.93	2.04/2.04/1.37	-
$\bar{P}_1^n$	5.98	7.15/7.11/7.18	6.66/6.50/6.64	-
$\bar{P}_2^n$	-5.98	-8.71/ - 8.04/ - 8.15	-7.46/ - 7.24/ - 7.87	-
$\bar{P}_3^n$	0.41	7.05/8.80/8.46	12.14/9.87/5.57	-
$\bar{D}^n$	-0.16	-0.12/ - / - 0.18	-	-

**Table 2.** Threshold values of the S-, P-, and D-wave multipoles for neutral pion photoproduction. Second column: pole contributions to the threshold multipoles. Third column: results of the unitary isobar model MAID03 [16], the dispersion analysis HDT [8], and the dynamical model DMT [17], in order. Fourth column: the predictions of HBChPT with the LECs given in Appendix B according to Refs. [11], [12], and [13]. The amplitudes  $E_{0+}$  are in units of  $10^{-3}/M_{\pi^+}$ , the P waves in units of  $10^{-3}/M_{\pi^+}^2$ , and the D waves in units of  $10^{-3}/M_{\pi^+}^3$ . The experimental data are from Ref. [14].

D waves contributes (see Eq. (23)), and according to Table 2 the non-pole contribution of these D waves is small. We clearly observe somewhat larger differences among the predictions for the neutron.

At this point we recall that the threshold of pion production moves to the origin of the Mandelstam plane ( $\nu = t = 0$ ) if we approach the soft pion limit. In order to get closer to this point we now study the dispersion integral of Eq. (36) as function of  $\nu$  at  $t = t_{\text{thr}}$ . This integral is an even function of  $\nu$ , and therefore it must have an extremum at  $\nu = 0$ . It is also very likely that the value of the integral decreases with decreasing  $\nu$ . However, the rapid decrease shown in Fig. 2 is astounding. The cusp effect at  $\nu = \nu_{\text{thr}}$  is very pronounced and leads to large deviations from the sum rule. However, the importance of the loop effects decreases rapidly if  $\nu$  moves to values below threshold. The correction vanishes at  $\nu \approx 70$  MeV, but because of the shallow minimum it is not possible to predict the zero-crossing precisely.

In the following Fig. 3 we display the integrands of the dispersion integrals for the isoscalar and isovector combinations. In the case of the isovector combination (lower panel), the contribution of the  $\Delta(1232)$  is dom-

inant. The cusp of threshold pion production is clearly seen for  $\nu = \nu_{\text{thr}}$ , however this effect reduces to a small shoulder below the  $\Delta$  resonance in the case of  $\nu = 0$ . The contribution of the second resonance region is small and practically independent of the choice of  $\nu$ . The isoscalar combination (upper panel) takes, of course, much smaller values than the isovector one. It also shows a strong cusp effect for  $\nu = \nu_{\text{thr}}$ , which rapidly decreases with smaller values of  $\nu$ . However, the integrand peaks in the region of the  $N^*(1520)$  and has some additional strength of the opposite sign in the third resonance region.

In Fig. 4 we investigate the convergence of the multipole expansion for the dispersion integral of the proton. The figure shows the dispersion integral (RHS of Eq. (36)) evaluated over a large energy range. The contribution to the integral value is clearly dominated by the imaginary part of the P-wave amplitude, but the S-wave contribution is substantial at low  $\nu$  values and yields the cusp effect at threshold. The imaginary parts of the higher partial waves turn out to be negligible over the whole energy region.

At this point the reader should recall that the dispersion relation is valid for the full invariant amplitudes  $A_i$ ,

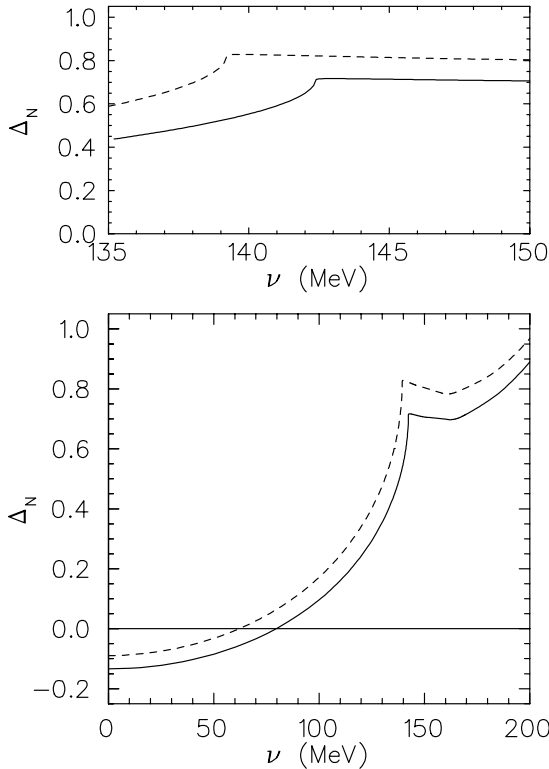


**Figure 2.** The correction to the FFR sum rule,  $\Delta_N(\nu, t_{\text{thr}})$ , as defined by Eq. (36) and obtained from the dispersion integral for proton (full line) and neutron (dashed line).

not for the multipoles individually. A decomposition of the real part of  $A_i$  into a multipole series looks quite different from Fig. 4, in that case the S wave provides the lion’s part of the amplitude in the region of  $\nu \lesssim 160$  MeV.

Figures 5 and 6 compare the predictions of HBChPT and DR for  $\Delta_N(\nu, t_{\text{thr}})$  as functions of  $\nu$  in the range  $0 \leq \nu \leq 200$  MeV, for the proton and the neutron, respectively. As we have seen before, all the predictions agree quite well in the threshold region (upper panels), which includes the cusp effect due to the opening of the charged pion channel.

There is also a reasonable agreement with the data points obtained by first inserting the experimental values of the multipoles (Ref. [14], see Table 2) in Eq. (22) and then subtracting the pole terms. As an example, the “experimental” threshold value has the following multipole decomposition:

$$\begin{aligned} \kappa_p + \Delta_p(\nu_{\text{thr}}, t_{\text{thr}}) &= 2.06 (S) + 0 (\bar{P}_1) \\ &+ 0.26 (\bar{P}_2) - 0.19 (\bar{P}_3) + 0.03 (\bar{D}) = 2.16. \end{aligned} \quad (37)$$

The result is clearly dominated by the S wave. However, the small total P-wave term comes about by a delicate cancellation among the P waves, which leads to a relatively large error bar for the FFR correction  $\Delta_N$  if calculated from the real part of the amplitude  $A_1$ . As we have seen in Figs. 3 and 4, the situation is quite different in the dispersive approach. In this case, the correction  $\Delta_N$  is essentially determined by  $\text{Im} M_{1+}$  in the region of the  $\Delta(1232)$  and a somewhat smaller contribution of  $\text{Im} E_{0+}$

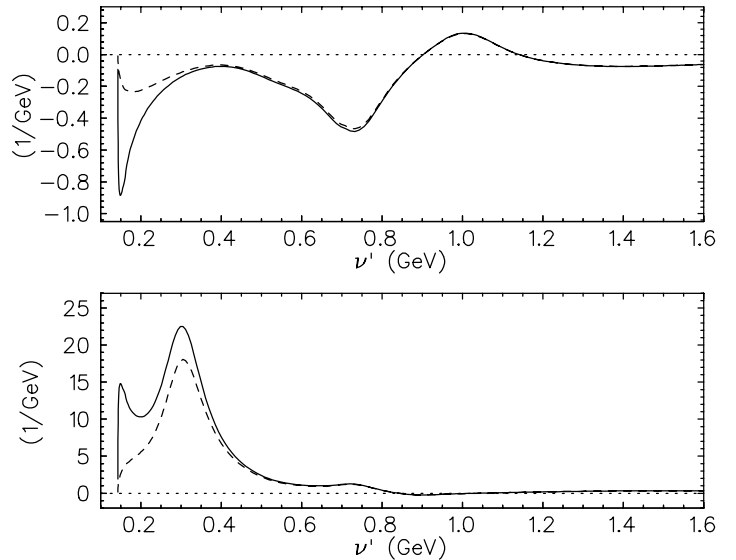


**Figure 3.** The integrands of the dispersion integrals (see RHS of Eq. (36)) for the isoscalar (top) and isovector (bottom) combinations of the amplitudes  $A_1$ . The full curves are obtained for  $\nu = \nu_{\text{thr}}$ , the dashed curves for  $\nu = 0$ .

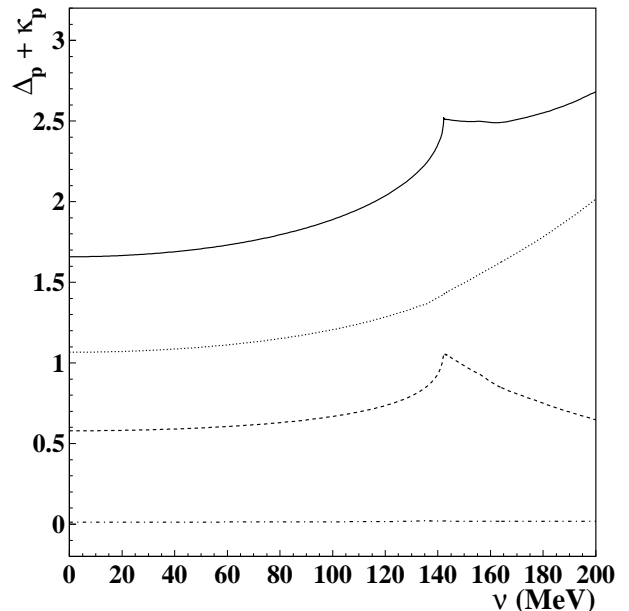


**Figure 4.** The values of  $\kappa_p + \Delta_p(\nu, t_{\text{thr}})$  obtained from the dispersion integral of Eq. (36) with a multipole decomposition of  $\text{Im} A_1$ . Solid line: full result for  $\text{Im} A_1$  evaluated with MAID03. Dashed line: results for the dispersion integral with only the S-wave contribution to  $\text{Im} A_1$ , dotted line: P-wave contribution only, dashed-dotted line: sum of D- and F-wave contributions.

in the threshold region. Both contributions are well under control and additive, and therefore the dispersive evaluation of  $\Delta_N$  should be quite stable.

Outside of the threshold region (lower panels), we observe 3 principal differences between HBChPT and the dispersive approach:

- (I) The rise of  $\Delta_N$  for  $\nu \gtrsim 170$  MeV is, of course, due to the  $\Delta(1232)$  resonance. It cannot be described by the “static” LECs of Appendix B, but will require a dynamical description of the resonance degrees of freedom as, e.g., in the “small scale expansion” [18]. Such effects could be approximately included by replacing the denominators  $(\Delta^2 - M_\pi^2)$  in the resonance contributions of Appendix B by  $(\Delta^2 - \omega^2)$ , which obviously leads to an enhancement of the resonance effects for  $\omega > M_\pi$ .
- (II) The curvature of the HBChPT predictions for small  $\nu$  is due to the nonrelativistic approach, which leads to (small) shifts of the nucleon pole positions. As may be seen from Eq. (22), the construction of the relativistic amplitude  $A_1$  requires that the multipole values be divided by factors of  $W - M_N$ , which vanish at the position of the s-channel pole  $\nu = \nu_B = -9.7$  MeV. It is therefore unavoidable that nonrelativistic approximations will lead to singularities at the s-channel pole, whereas the u-channel pole at  $\nu = -\nu_B = 9.7$  MeV does not show up because of the angular integration involved in the multipole expansion of Eq. (22). As a consequence nonrelativistic expansions are bound to yield large violations of crossing symmetry in the region of small  $\nu$  values.
- (III) Except for the differences mentioned above, the predictions of Refs. [11] and [12] are in qualitative agreement with the result of the dispersion approach as shown in Figs. 5 and 6. However, the prediction of Ref. [13] leads to a practically constant value of  $\Delta_p \approx 0.55$  for  $\nu < \nu_{\text{thr}}$ . The reason for this difference is almost entirely due to the additionally included  $\mathcal{O}(q^4)$  loop terms in the P waves. Whereas this term is essentially cancelled in  $\bar{P}_2$  by a similarly large counterterm, the cancellation is less effective for  $\bar{P}_1$ . As we note from Eq. (23), this fact does not show up near threshold where  $\bar{P}_1$  does not contribute to the amplitude  $A_1$ .

The description of pion photoproduction by HBChPT was preceded by a relativistic calculation at the one-loop order [15], which revised an old low-energy theorem and explained the strong suppression of neutral pion photoproduction on the proton by loop effects. Unfortunately, it was then not possible to define a systematic power counting underlying such a relativistic field theory if nucleons were involved. This problem could be solved by HBChPT, which organizes the Lagrangian as a power series in  $1/M_N$  in order to obtain a well-defined expansion of the observables if the typical external momenta of the system are small compared to the nucleon mass. As we have seen above, HBChPT can indeed well describe the amplitudes in the threshold region, whereas it fails in the region of small  $\nu$  values. Because of its non-relativistic approximations, it misses the nucleon pole positions and thus fails to reproduce the crossing-symmetry, which is one of the essentials of a dispersive approach. The shortcomings of HBChPT have of course been noted often before, and several groups are now working to apply the newly developed manifestly Lorentz-invariant renormalization schemes [19] to various physical processes, in particular also to pion

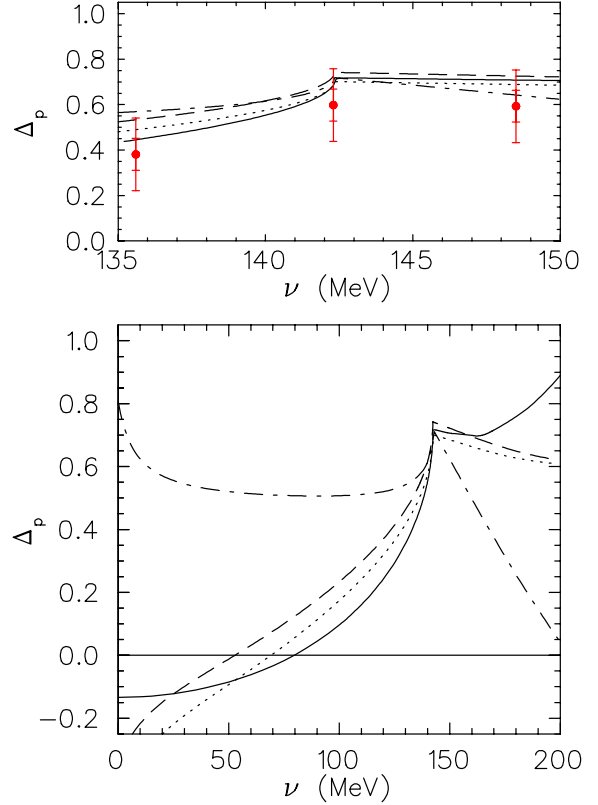


**Figure 5.** The correction to the FFR sum rule for the proton,  $\Delta_p(\nu, t_{\text{thr}})$  as defined by Eqs. (35) and (36). A comparison of the dispersive approach (solid lines) with the predictions of HBChPT, represented by the dotted [11], dashed [12], and dashed-dotted [13] lines. The data points are calculated with the experimental S- and P-wave multipoles of Ref. [14].

photoproduction. However, the general structure of the dispersive part of the amplitude  $A_1$  for small external momenta has already been given in Ref. [15]:

$$A_1^{\text{disp}} = a_{00} + a_{02}\nu_B + a_{20}\nu^2 + \dots, \quad (38)$$

where the coefficients  $a_{ik}$  are functions of the mass ratio  $\mu = M_\pi/M_N$ . In particular the leading coefficients depend on the pion mass as follows:  $a_{00} = \mathcal{O}(\mu^2)$ ,  $a_{02} = \mathcal{O}(\ln \mu)$ , and  $a_{20} = \mathcal{O}(\mu^{-1})$ . The vanishing of  $a_{00}$  in the chiral limit is, of course, a necessary condition for the validity of the FFR sum rule. Furthermore, the divergence of the higher expansion coefficients in that limit is the reason why the old low-energy theorem for neutral pion photoproduction failed.

Since the FFR discrepancy  $\Delta_N(\nu, t)$  is directly related to  $A_1^{\text{disp}}$ , it has a power series expansion similar to Eq. (38),

$$\Delta_N(\nu, t) = \delta_{00}^N + \delta_{02}^N \frac{t - M_\pi^2}{4M_N} + \delta_{20}^N \nu^2 + \dots \quad (39)$$

In particular  $\delta_{00}$  can be determined by an analytical continuation of the multipole expansion of Eq. (18) to the

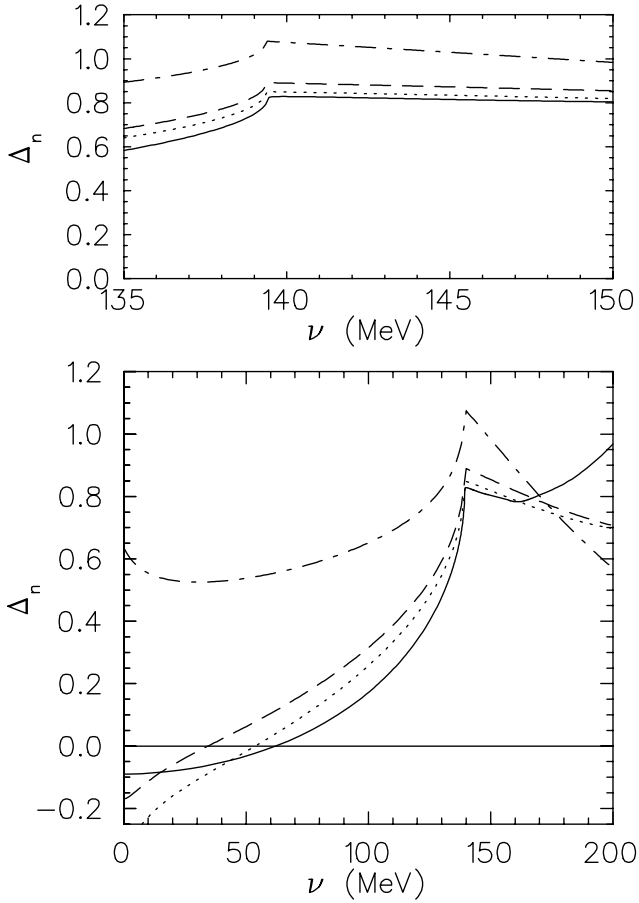


**Figure 6.** The correction to the FFR sum rule for the neutron,  $\Delta_n(\nu, t_{\text{thr}})$  as defined by Eqs. (35) and (36). A comparison of the dispersive approach (solid lines) with the predictions of HBChPT, represented by the dotted [11], dashed [12], and dashed-dotted [13] lines.

unphysical point ( $s = u = M_N^2$ ,  $t = M_\pi^2$ ) at which all particles are on their mass shell (see Fig. 1), i.e.,

$$\delta_{00}^N = \Delta_N(\nu = 0, t = M_\pi^2). \quad (40)$$

This extrapolation requires some care, because the Legendre polynomials  $P_\ell(x)$  involved in the expansion have to be evaluated at  $|x| > 1$ . However, preliminary studies with only S- and P-wave contributions indicate that  $\delta_{00}^N$  is small. The remaining two constants in Eq. (39) can be approximately obtained by DRs at  $t = t_{\text{thr}}$ , in which case the path of integration is fully contained in the physical region. The value of  $\delta_{02}^N$  can be read off at  $\nu = 0$ ,

$$\delta_{02}^N \approx \frac{4M_N}{t_{\text{thr}} - M_\pi^2} (\Delta_N(\nu = 0, t_{\text{thr}}) - \delta_{00}^N), \quad (41)$$

where the ellipses denote the influence of higher order terms as in Eq. (39). The coefficients of  $\nu^{2n}$ ,  $n \geq 1$ , can be easily obtained by expanding the dispersion integral of Eq. (36), e.g.,

$$\delta_{2n,0}^N \approx \frac{4M_N^2}{\pi e g_{\pi N}} \int_{\nu_{\text{thr}}}^{\infty} \frac{d\nu'}{(\nu')^{2n+1}} \text{Im} A_1^{(N,\pi^0)}(\nu', t_{\text{thr}}). \quad (42)$$

Due to the additional factors of  $1/\nu'^2$ , these integrals are well saturated by the threshold and  $\Delta(1232)$  resonance regions. The numerical results for these coefficients are  $\delta_{20}^p = 0.368/M_{\pi^+}^2$ ,  $\delta_{40}^p = 0.120/M_{\pi^+}^4$ , and  $\delta_{60}^p = 0.054/M_{\pi^+}^6$ , and Fig. 7 shows the convergence of the respective Taylor series below pion threshold.

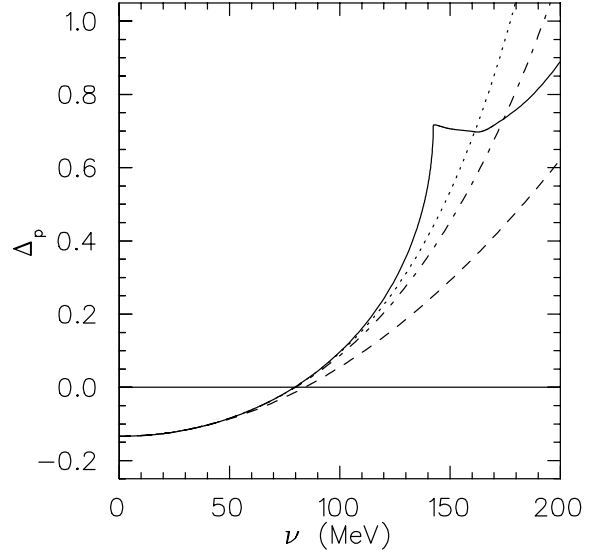


**Figure 7.** Full line: the correction  $\Delta_p(\nu, t_{\text{thr}})$  as defined by Eq. (36), compared to the low-energy expansion in the crossing-symmetrical variable  $\nu$ . Dashed line: term of  $\mathcal{O}(\nu^2)$ , dashed-dotted line: up to  $\mathcal{O}(\nu^4)$ , and dotted line: up to  $\mathcal{O}(\nu^6)$ .

## 5 Summary and Outlook

The Furbini-Fulan-Rossetti (FFR) sum rule connects the nucleon's anomalous magnetic moment with the neutral pion photoproduction amplitudes  $A_1^{(+,0)}(\nu, t)$  in the chiral limit of massless pions. We have studied the finite mass corrections to this sum rule in the framework of dispersion relations at  $t = \text{const}$  as function of the crossing-symmetrical variable  $\nu$ . The path of integration has been chosen such that it passes through the threshold of pion photoproduction,  $\nu = \nu_{\text{thr}}$  and  $t = t_{\text{thr}}$ , because this is the only  $t$ -value for which the integrand of the DR is fully contained in the physical region. A comparison with the results of heavy baryon chiral perturbation theory (HBChPT) shows excellent agreement in the threshold region but deviations for both higher and lower energies. For energies moving towards the  $\Delta(1232)$  resonance, the agreement can be improved by including the dynamical degrees of freedom of that resonance as, e.g., in the “small scale expansion”. For energies far below threshold, the problem lies in the nonrelativistic approximations involved in HBChPT. As a consequence of these approximations, the nucleon poles are situated at the wrong positions, which leads to singularities in the dispersive amplitude and to a violation of the crossing symmetry. The

remedy for these problems lies in a manifestly Lorentz-invariant treatment of pion photoproduction, which at the same time should also provide a systematic expansion scheme. This challenge has prompted several groups to take up the issue, and a solution of the problem is to be expected soon.

The aim of our work is two-fold. First, we want to put our phenomenological model MAID on a dispersive basis, i.e., the real and imaginary parts of the pion production amplitudes should be Hilbert transforms of each other. The obvious technique to connect these amplitudes are DRs at  $t = \text{const}$ , which in general requires an integration over physical and unphysical regions. The present version of MAID03 involves all four-star S-, P-, D-, and F-wave resonances up to total c.m. energy  $W = 2$  GeV, and the convergence problem of the multipole series in the unphysical region has to be studied with great care. In this sense we see the FFR sum rule as a good testing ground for the development of a ‘‘dispersion MAID’’.

The second aim of our work is to connect the dispersive approach to the soon expected results from relativistic ChPT. The low-energy constants (LECs) of such a theory can be provided by dispersion integrals that contain global properties of the resonance spectrum. Since these LECs are the coefficients of a power series in small  $\nu$ ,  $t$ , and  $M_\pi$ , the ideal meeting ground between relativistic ChPT and DRs is in the unphysical region around the origin of the Mandelstam plane,  $\nu = t = 0$ .

In our work we have concentrated on the FFR sum rule and the amplitudes  $A^{(+,0)}$  for neutral pion photoproduction. It will be straightforward to extend our approach to charged pion photoproduction and, eventually, to all 6 amplitudes of pion electroproduction. We hope that this future work will provide many new cross-checks with relativistic effective field theories, improve our understanding of pion production as the most prominent decay mode of the nucleonic resonance spectrum, and lead to new insights concerning the interplay between pion-cloud and resonance structure of the nucleon.

## Acknowledgements

The authors gratefully acknowledge several discussions with Norbert Kaiser and Ulf-G. Meißner on various aspects of Chiral Perturbation Theory. This work was supported by the Italian MIUR through the PRIN Theoretical Physics of the Nucleus and the Many-Body Systems (B. Pasquini) and by the Deutsche Forschungsgemeinschaft (SFB 443). This research is part of the EU Integrated Infrastructure Initiative Hadron Physics Project under contract number RII3-CT-2004-506078.

## Appendix

### A Pole contribution

The pole contribution to the S- and P-wave multipoles at threshold can be derived from the invariant amplitudes

given in Eq. (15),

$$\begin{aligned}
E_{0+}(\omega_{thr}) &= \frac{\mu M_N}{8\pi} \frac{2 + \mu}{(1 + \mu)^{3/2}} \\
&\quad \left[ A_1 + \mu M_N \frac{2 + \mu}{2(1 + \mu)} A_3 + \frac{\mu^2 M_N}{2(1 + \mu)} A_4 \right], \\
\bar{P}_2(\omega_{thr}) &= \frac{\mu}{16\pi} \frac{(2 + \mu)}{(1 + \mu)^{3/2}} \\
&\quad \left[ -A_1 + 2\mu M_N^2 A_2 + \frac{M_N(2 + \mu)^2}{2(1 + \mu)} \right. \\
&\quad \left. A_3 + \mu M_N \frac{2 + \mu}{2(1 + \mu)} A_4 \right], \\
\bar{P}_3(\omega_{thr}) &= \frac{\mu}{16\pi} \frac{2 + \mu}{(1 + \mu)^{3/2}} \\
&\quad \left[ -A_1 + \frac{\mu^2 M_N}{2(1 + \mu)} A_3 + M_N \frac{4 + 6\mu + \mu^2}{2(1 + \mu)} A_4 \right],
\end{aligned} \tag{43}$$

where  $\mu = M_\pi/M_N$  and  $A_i = A_i(s_{thr}, t_{thr})$ . The threshold values of the latter amplitudes follow from Eq. (15):

$$\begin{aligned}
A_1^{\text{pole}} &= -\frac{1 + \tau_3}{2} \frac{eg_{\pi N}}{M_N^2} \frac{1}{(2 + \mu)}, \\
A_2^{\text{pole}} &= -(1 + \tau_3) \frac{eg_{\pi N}}{M_N^4} \frac{(1 + \mu)}{\mu^2(2 + \mu)^2}, \\
A_3^{\text{pole}} &= -\tau_3 \kappa_N \frac{eg_{\pi N}}{2M_N^3 \mu}, \\
A_4^{\text{pole}} &= \tau_3 \kappa_N \frac{eg_{\pi N}}{2M_N^3} \frac{1}{(2 + \mu)}.
\end{aligned} \tag{44}$$

The threshold values of the 3 multipoles given by Eqs. (43) can be directly obtained by inserting the threshold amplitudes of Eqs. (44). In the case of  $\bar{P}_1^{\text{pole}}(\omega_{thr})$ , we first have to project out the P-wave content of the invariant amplitudes before going to the threshold kinematics. As a result the pole contributions to the S- and P-wave multipoles take the form

$$\begin{aligned}
E_{0+}^{\text{pole}}(\omega_{thr}) &= -\frac{eg_{\pi N}}{8\pi M_N} \frac{\mu}{(1 + \mu)^{3/2}} \left[ \frac{1 + \tau_3}{2} + \tau_3 \kappa_N \right], \\
\bar{P}_1^{\text{pole}}(\omega_{thr}) &= \frac{eg_{\pi N}}{16\pi M_N^2} \frac{2 + \mu}{(1 + \mu)^{3/2}} \left[ \frac{1 + \tau_3}{2} + \tau_3 \kappa_N \right], \\
\bar{P}_2^{\text{pole}}(\omega_{thr}) &= -\frac{eg_{\pi N}}{16\pi M_N^2} \frac{2 + \mu}{(1 + \mu)^{3/2}} \\
&\quad \left[ \frac{1 + \tau_3}{2} \left( 1 - \frac{2\mu(1 + \mu)}{(2 + \mu)^2} \right) + \tau_3 \kappa_N \right], \\
\bar{P}_3^{\text{pole}}(\omega_{thr}) &= \frac{eg_{\pi N}}{16\pi M_N^2} \frac{\mu}{(1 + \mu)^{3/2}} \left[ \frac{1 + \tau_3}{2} + \tau_3 \kappa_N \right].
\end{aligned} \tag{45}$$

The FFR contributions are obtained by evaluating Eq. (25) at threshold:

$$E_{0+}^{\text{FFR}}(\omega_{thr}) = \frac{eg_{\pi N} \tau_3 \kappa_N}{16\pi M_N} \frac{\mu(2 + \mu)}{(1 + \mu)^{3/2}}, \tag{46}$$

$$\begin{aligned}\bar{P}_1^{\text{FFR}}(\omega_{thr}) &= -\bar{P}_2^{\text{FFR}}(\omega_{thr}) = -\bar{P}_3^{\text{FFR}}(\omega_{thr}) \\ &= \frac{eg_{\pi N} \tau_3 \kappa_N}{32\pi M_N^2} \frac{\mu(2+\mu)}{(1+\mu)^{3/2}}.\end{aligned}$$

The sum of Eqs. (45) and (46) yields the result of pseudo-vector pion-nucleon coupling, which agrees with the expansion of Refs. [11,13] up to  $\mathcal{O}(1/M_N^4)$ .

## B Low energy constants of HBChPT

In the following we list the low-energy constants determined by several investigations on neutral pion photoproduction off the proton.

(I) Resonance fit of Ref. [11]:

The low-energy constants (LECs) are obtained by the resonance saturation principle. The t-channel exchange of the vector mesons  $\rho(770)$  and  $\omega(782)$  leads to:

$$\begin{aligned}a_1^V &= -\frac{1}{24\pi^3 M_N F_\pi^3}, \\ a_2^V &= \frac{5}{48\pi^3 M_N F_\pi^3}, \\ b_P^V &= \frac{5}{64\pi^3 F_\pi^3},\end{aligned}\quad (47)$$

where  $F_\pi = 93$  MeV has been used. The largest resonance contribution in the s-channel is given by  $\Delta(1232)$  excitation. The corresponding contribution  $a_1^\Delta$ ,  $a_2^\Delta$  and  $b_P^\Delta$  were determined according to Eqs. (4.8)-(4.9) of Ref. [11] with the following parameters:  $C = 0.40$  GeV<sup>-5</sup>,  $g_1 = g_2 = 5$ ,  $X = 2.24$ ,  $Y = 0.13$ ,  $Z = 0.28$ . The resulting values are:  $a_1^\Delta = 1.26$  GeV<sup>-4</sup>,  $a_2^\Delta = 2.62$  GeV<sup>-4</sup>,  $b_P^\Delta = 12.75$  GeV<sup>-3</sup>. The LECs of model (I) were then obtained by adding the s- and t-channel contributions:  $a_1 = -0.52$  GeV<sup>-4</sup>,  $a_2 = 7.07$  GeV<sup>-4</sup>,  $b_P = 15.88$  GeV<sup>-3</sup>.

(II) Resonance fit of Ref. [12]:

The LECs follow from the same procedure as above except for different values of the off-shell parameters of  $\Delta$  excitation,  $X = 2.75$ ,  $Y = 0.10$ ,  $Z = -0.21$ . The result is  $a_1 = (-1.78 + 2.46)$  GeV<sup>-4</sup> = 0.68 GeV<sup>-4</sup>,  $a_2 = (4.45 + 1.45)$  GeV<sup>-4</sup> = 5.90 GeV<sup>-4</sup>,  $b_P = (3.13 + 9.89)$  GeV<sup>-3</sup> = 13.03 GeV<sup>-3</sup>, where the first values in the brackets refer to the vector meson, the second value to the  $\Delta$  contribution.

(III) Five-parameter fit of Ref. [13]:

This calculation includes both S- and P-waves consistently to fourth order in HBChPT. The S-wave LECs are taken from a comparison with differential cross sections and photon asymmetries (Set II of Table 2 in Ref. [13]),  $a_1 = 8.588$  GeV<sup>-4</sup>,  $a_2 = -2.288$  GeV<sup>-4</sup>, while the 3 P-wave LECs follow from resonance saturation,

$$b_P^V = \frac{5}{64\pi^3 F_\pi^3}, \quad \xi_1^V = -\frac{8}{g_A}, \quad \xi_2^V = \frac{4}{g_A}, \quad (48)$$

with  $F_\pi = 92.4$  MeV and  $g_A = g_{\pi N} F_\pi / M = 1.29$ . The  $\Delta$  contributions are determined from

$$\begin{aligned}b_P^\Delta &= \frac{\kappa^* g_A}{6\sqrt{2}\pi M_N F_\pi} \frac{\Delta}{\Delta^2 - M_\pi^2}, \\ \xi_1^\Delta &= -\xi_2^\Delta = \frac{\kappa^*}{3\sqrt{2}} \frac{16\pi^2 F_\pi^2}{\Delta^2 - M_\pi^2},\end{aligned}\quad (49)$$

where  $\Delta$  is the  $N\Delta$  mass splitting and  $\kappa^*$  the  $N\Delta$  transition magnetic moment. With  $\Delta = 293$  MeV and  $\kappa^* = 4.86$ , the total result for the LECs is

$$\begin{aligned}b_P &= (3.19 + 11.73) \text{ GeV}^{-3} = 14.93 \text{ GeV}^{-3}, \\ \xi_1 &= -6.21 + 22.84 = 16.63, \\ \xi_2 &= 3.10 - 22.84 = -19.73.\end{aligned}\quad (50)$$

The LECs for the neutron differ from those of the proton in the vector meson contributions according to

$$a_i^{V,n} = \frac{1}{8} a_i^{V,p}, \quad b_P^{V,n} = \frac{4}{5} b_P^{V,p}, \quad \xi_1^{V,n} = \frac{1}{8} \xi_1^{V,p}, \quad (51)$$

while the  $\Delta$  resonance contributions remain unchanged.

## References

1. S. Fubini, G. Furlan, and C. Rossetti, Nuovo Cim. 40 (1965) 1171.
2. M. Goldberger and S. Treiman, Phys. Rev. 110 (1958) 1478.
3. S. Fubini, C. Rossetti, and F. Furlan, Nuovo Cim. 43A (1966) 161.
4. S.L. Adler and F.J. Gilman, Phys. Rev. 152 (1966) 1460.
5. W. Schmidt and G. Höhler, Ann. Phys. (N.Y.) 28 (1964) 34; N. Schmidt, Z. Physik 182 (1964) 76.
6. R.A. Arndt and R.L. Workman, nucl-th/9503002; R.A. Arndt, I.I. Strakovsky, and R.L. Workman, Phys. Rev. C 53 (1996) 430.
7. G.F. Chew et al., Phys. Rev. 106 (1957) 1345.
8. O. Hanstein, D. Drechsel, and L. Tiator, Nucl. Phys. A 632 (1998) 561.
9. J.D. Bjorken and S.D. Drell, "Relativistic quantum fields", (McGraw-Hill, New York, 1965).
10. J.S. Ball, Phys. Rev. 124 (1961) 2014.
11. V. Bernard, N. Kaiser, and Ulf-G. Meißner, Z. Phys. C 70 (1996) 483.
12. V. Bernard, N. Kaiser, and Ulf-G. Meißner, Phys. Lett. B 378 (1996) 337.
13. V. Bernard, N. Kaiser, and Ulf-G. Meißner, Eur. Phys. J. A 11 (2001) 209.
14. A. Schmidt et al., Phys. Rev. Lett. 87 (2001) 232501.
15. V. Bernard, N. Kaiser, and Ulf-G. Meißner, Phys. Lett. B 268 (1991) 291; Nucl. Phys. B 383 (1992) 442.
16. D. Drechsel, O. Hanstein, S.S. Kamalov, L. Tiator, Nucl. Phys. A 645 (1999) 145; <http://www.kph.uni-mainz.de/MAID/>.
17. S.S. Kamalov, G.-Y. Chen, S.N. Yang, D. Drechsel, L. Tiator, Phys. Lett. B 522 (2001) 27.

18. T.R. Hemmert, B.R. Holstein, and J. Kambor, Phys. Rev. D 55 (1997) 5598; V. Bernard, H.W. Fearing, T.R. Hemmert, and U.-G. Meißner, Nucl. Phys. A 635 (1998) 121 and A 642 (1998) 563.
19. T. Becher and H. Leutwyler, Eur. Phys. C 9 (1999) 643; B. Kubis and U.-G. Meißner, Nucl. Phys. A 679 (2001) 698; T. Fuchs, J. Gegelia, G. Japaridze, and S. Scherer, Phys. Rev. D 68 (2003) 056005.